Nanocomposites

DOI: 10.1002/anie.201402751

In Situ Synthesis of Robust Conductive Cellulose/Polypyrrole Composite Aerogels and Their Potential Application in Nerve Regeneration**

Zhuqun Shi, Huichang Gao, Jiao Feng, Beibei Ding, Xiaodong Cao, Shigenori Kuga, Yingjun Wang, Lina Zhang, and Jie Cai**

Abstract: *Nanostructured conductive polymers can offer analogous environments for extracellular matrix and induce cellular responses by electric stimulation, however, such materials often lack mechanical strength and tend to collapse under small stresses. We prepared electrically conductive nanoporous materials by coating nanoporous cellulose gels (NCG) with polypyrrole (PPy) nanoparticles, which were synthesized in situ from pyrrole monomers supplied as vapor. The resulting NCG/PPy composite hydrogels were converted to aerogels by drying with supercritical CO_2, giving a density of 0.41–0.53 $g\,cm^{-3}$, nitrogen adsorption surface areas of 264–303 $m^2\,g^{-1}$, and high mechanical strength. The NCG/PPy composite hydrogels exhibited an electrical conductivity of up to 0.08 $S\,cm^{-1}$. In vitro studies showed that the incorporation of PPy into an NCG enhances the adhesion and proliferation of PC12 cells. Electrical stimulation demonstrated that PC12 cells attached and extended longer neurites when cultured on NCG/PPy composite gels with DBSA dopant. These materials are promising candidates for applications in nerve regeneration, carbon capture, catalyst supports, and many others.*

Conductive polymers such as polyaniline (PANI), polypyrrole (PPy), and their derivatives have been used to prepare advanced materials, such as dye-sensitized solar cells,[1] energy storage materials,[2] sensors,[3] and materials for water treatment[4] and CO_2 capture,[5] because of their facile synthesis and flexibility in processing.[6] In particular, nanoporous PPy architectures can offer environments analogous to an extracellular matrix and induce cellular responses by electric stimulation.[7] The exploitation of nanostructured conductive polymers, is however hampered by their low solubility, poor mechanical integrity, and difficulty in fabrication. Several attempts to facilitate their fabrication have been investigated, utilizing biomacromolecules as template in in situ polymerization and blending approaches; examples of templates include cellulose,[8] alginate,[9] gellan gum,[10] and DNA.[11]

Among these templates, cellulose attracted special attention because of its remarkable physical properties, such as a high elastic modulus of 100–200 GPa compared to carbon nanotubes,[12] and a low thermal expansivity of 0.1 ppm K^{-1} compared to silica,[13] and its sustainability and availability at low cost. Nanoporous cellulose gels (NCG) prepared from aqueous alkali/urea solutions showed remarkable mechanical strength and light transmittance.[14] They were characterized by a high porosity with open-pore structures, and were thus used effectively for the synthesis of metallic or nonmetallic nanoparticles.[15] They were also used for the preparation of mechanically tough, foldable, and transparent cellulose bioplastics.[16]

Here we present preliminary but remarkable results demonstrating the in situ synthesis of PPy in an NCG matrix. While the polymerization of pyrrole can be accomplished by an electrolytic method or through oxidative initiation,[17] the latter is suitable for our purpose of an in situ synthesis in a gel template. The polymerization was achieved by simply mixing pyrrole monomers with oxidants, typically ferric salts, in a liquid phase. To avoid polymerization outside the gel, we employed the vapor-phase method, which has been applied previously to the coating of nanofibers with PPy.[18] The resulting NCG/PPy composite gels were dried using supercritical CO_2 to give aerogels with a low density, a large surface area, high mechanical integrity, sufficient electrical conductivity, and no cytotoxicity. A PC12 cell line was used to evaluate the biological performance of the composites for potential biomedical applications in nerve regeneration.

Figure 1 describes the synthesis of the aerogels. The NCG hydrogel was transparent, colorless, and flexible, with a water content of 92% and a porosity of 95%. The liquid in the gel was exchanged with ethanol (giving the alcogel) and impregnated with a solution of $FeCl_3$ in ethanol. After the removal of

[*] Z. Shi,[+] J. Feng, B. Ding, Prof. L. Zhang, Prof. J. Cai
College of Chemistry & Molecular Sciences, Wuhan University
Wuhan, 430072 (China)
E-mail: caijie@whu.edu.cn
jiecaiwhu@hotmail.com
H. Gao,[+] Prof. X. Cao, Prof. Y. Wang
School of Materials Science and Engineering
South China University of Technology
Guangzhou, 510641 (China)
E-mail: caoxd@scut.edu.cn
Prof. S. Kuga
Graduate School of Agricultural and Life Sciences
The University of Tokyo (Japan)
[+] These authors contributed equally to this work.

[**] This work was supported by the National Basic Research Program of China (973 Program, 2010CB732203, 2012CB619100), the National Natural Science Foundation of China (51373125, 20904043, 51372085), and the State Key Program of National Natural Science of China (21334005).

Supporting information for this article is available on the WWW under http://dx.doi.org/10.1002/anie.201402751.

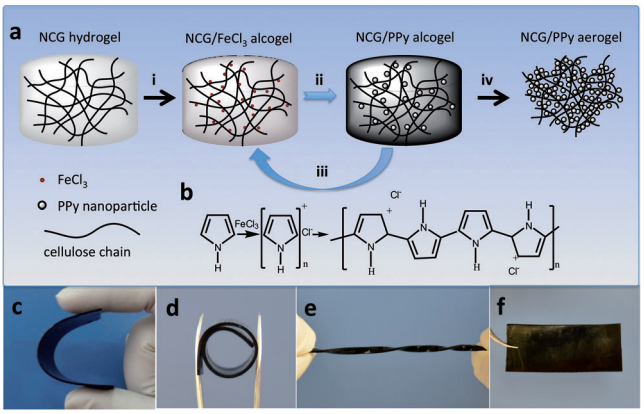

Figure 1. a) Preparation of NCG/PPy composite aerogels. 1) The NCG hydrogel with interconnected nanofibrillar network is solvent-exchanged with ethanol, and then impregnated with a solution of $FeCl_3$ in ethanol to form the NCG/$FeCl_3$ alcogel. 2) PPy nanoparticles are formed by in situ vapor-phase polymerization of pyrrole monomers supplied as vapor, giving the NCG/PPy-1 composite alcogel. 3) Repeating the second step two or three times gives NCG/PPy-2 and NCG/PPy-3 composite alcogels, respectively. 4) Drying with supercritical CO_2 gives NCG/PPy composite aerogel. b) Schematic representation of pyrrole polymerization with $FeCl_3$. Macroscopic views of NCG/PPy-3 composite hydrogels under c) bending (63 mm × 28 mm × 0.9 mm), d) rolling (internal diameter of 10 mm), and e) torsional loading (63 mm × 5 mm × 0.9 mm), and f) NCG/PPy-3 composite aerogel (63 mm × 28 mm × 0.9 mm).

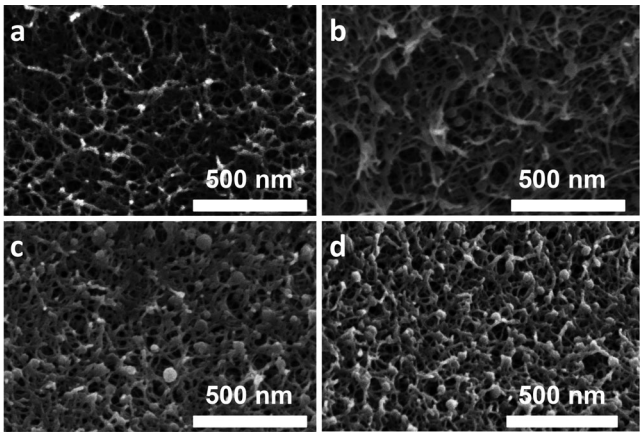

Figure 2. Scanning electron microscopy (SEM) images of the cross-section of the a) NCG, b) NCG/PPy-1, c) NCG/PPy-2, and d) NCG/PPy-3 composite aerogels.

excess liquid from the surface, the gel sheet was subjected to in situ vapor-phase polymerization of pyrrole monomers in the NCG matrix (Figure 1b). After 12 hours in pyrrole vapors, the gel sheet turned black as a result of the formation of PPy. This procedure was repeated three times to obtain three levels of PPy content. The NCG/PPy composite gel was rinsed with deionized water, solvent-exchanged with ethanol, and then converted to the aerogel by drying with supercritical CO_2. While the NCG/PPy composite hydrogels demonstrated good mechanical stability under bending, rolling, and torsional loading (Figure 1c–e), its aerogel was robust (Figure 1f).

The FT-IR spectrum of the NCG/PPy composite aerogel shows the superposition of characteristic peaks of the NCG and PPy (see Figure S1 in the Supporting Information), thus confirming the polymerization of pyrrole in the NCG.[19] We observed that the O-H stretching absorption peak of the NCG at 3340 cm^{-1} and the antisymmetric ring stretching absorption peak of the PPy at 1543 cm^{-1} shift to 3312 and 1560 cm^{-1}, respectively, in the composite aerogel, thus indicating that the N-H groups of the pyrrole rings form hydrogen bonds with the hydroxy groups of cellulose.[20]

The PPy content of the composite increased from 25 to 57 wt% by repeating the 12 hour long vapor-phase polymerization cycles (Table 1). The SEM image of the NCG aerogel (Figure 2a) shows a mesoporous structure composed of interconnected cellulose nanofibrils. The typical diameter of the cellulose nanofibrils is less than 10 nm, agreeing well with the Brunauer–Emmett–Teller (BET) surface area of 356 $m^2 g^{-1}$, determined by nitrogen adsorption (Table 1), which translates to a fibril width of 7 nm. The SEM images of NCG/PPy composite aerogels (Figure 2b–d) show the features of PPy deposition. PPy appears as spherical nanoparticles with diameters of 30–60 nm, with an increasing population of nanoparticles after increased polymerization times. At the same time, the fibrils that form the network seem gradually thickened; therefore PPy likely forms a continuous coating layer on the cellulose. These features are more clearly observable in TEM images of ultrathin sections (Figure 3). The TEM images verify that the PPy nanoparticles are spherical and have diameters of 40–60 nm. The PPy nanoparticles dispersed well in the NCG matrix, which is very useful for their stable dispersion (Figure 3a,b). After three polymerization cycles, the individual PPy nanoparticles connected and formed a nanoporous interconnected network (Figure 3c,d).

Table 1: Physical properties of the NCG and NCG/PPy composite hydrogels and aerogels.

Sample	Elemen. anal.			Porosity	Conductivity	Density	BET	Hydrogel			Aerogel			Comp.
	C [wt%]	N [wt%]	PPy [wt%]	[%]	[S cm^{-1}]	[g cm^{-3}]	[$m^2 g^{-1}$]	σ_b [MPa]	ε_b [%]	E [MPa]	σ_b [MPa]	ε_b [%]	E [MPa]	mod. [MPa]
NCG	44	0	0	93	–	0.14	356	3.7	66	5.3	5.7	26	127	62
NCG/PPy-1	43	4.4	25	74	–	0.41	303	3.1	41	6.2	4.1	3.3	203	64
NCG/PPy-2	49	7.0	37	73	1×10^{-5}	0.43	264	1.8	30	6.3	3.8	2.8	245	72
NCG/PPy-3	49	9.8	57	66	0.08	0.53	276	1.3	23	8.1	3.6	2.0	197	164

σ_b, ε_b, and E are the tensile strength, elongation at break, and Young's modulus of hydrogels and aerogels under stretching model, respectively. BET = BET surface area, Comp. mod. = compression modulus.

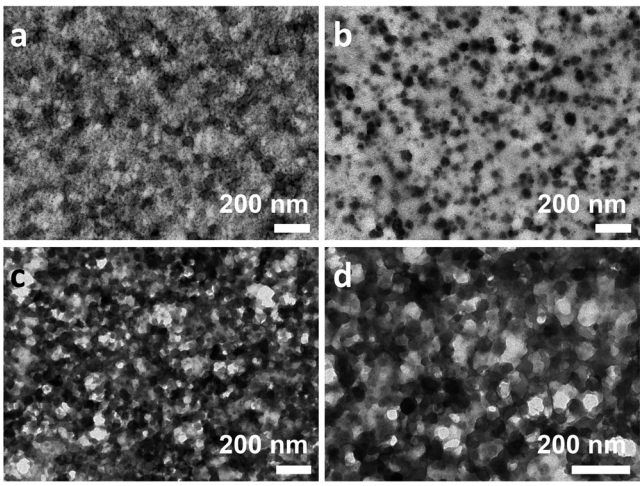

Figure 3. Transmission electron microscopy (TEM) images of the a) NCG/PPy-1, b) NCG/PPy-2, and c,d) NCG/PPy-3 composite aerogels. (d) is the higher magnification image of (c).

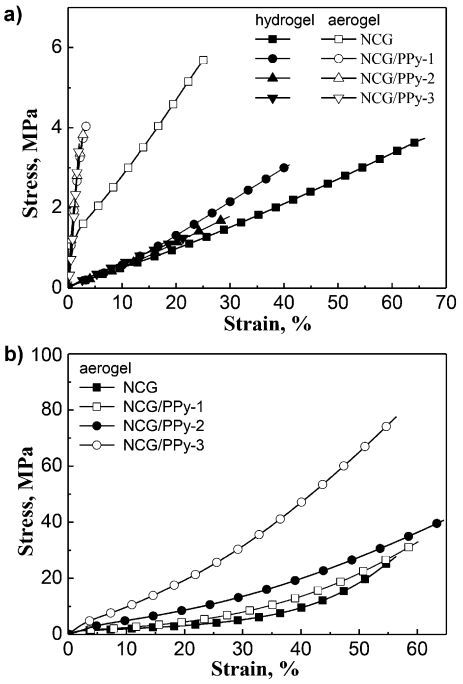

Figure 4. Stress–strain curves of the NCG and NCG/PPy composite hydrogels and aerogels under stretching (a) and compression (b) models.

The nitrogen adsorption isotherms for the composite aerogels were of IUPAC type IV (see Figure S2 in the Supporting Information). The increased PPy content did not have a remarkable influence on the porous structure of the aerogels, but resulted in a moderate decrease of the BET surface area from 356 $m^2 g^{-1}$ to 264 $m^2 g^{-1}$ and the porosity from 93% to 66% (Table 1). The Barrett–Joyner–Halendar (BJH) analysis indicated that the composite aerogels had larger mesopores, approximately 25 nm at peak maximum, than those of the original cellulose aerogel, approximately 18 nm; furthermore the total volume of the mesopores was doubled. This result is consistent with the theoretical evidence for an increase in the mean pore size with an increase in the fiber diameter.[21]

The X-ray diffraction patterns of composite aerogels (see Figure S3 in the Supporting Information) are a nearly systematic superposition of those of the neat NCG and PPy, thus indicating no interference in structure formation between the components. These results, together with the results from electron microscopy analyses, gave a consistent picture, that is, the NCG/PPy composite gel is macroscopically homogeneous, but consists of microscopically separated composites, thus resulting in the superposition of properties of the two components.

These spectral and morphological characteristics indicate that the synthesized PPy nanoparticles are fixed on the surface of cellulose nanofibers and form a continuous layer along the cellulose nanofibers. This nanoscale hybridization was achieved by in situ vapor-phase polymerization, that is, PPy formed in the finely divided space cannot grow into large particles or aggregates, but are forced to deposit on cellulose nanofibrils nearby. It is likely that initially formed oligomers attach to the gel network and act as nucleus for polymer deposition.[22]

The tensile behavior of the composite hydrogels changed gradually by the addition of PPy (Figure 4a); tensile strength (σ_b) and elongation at break (ε_b) of the NCG/PPy hydrogels decreased from 3.7 MPa to 1.3 MPa and 66% to 23%, respectively, with an increasing PPy content from 25 wt% to 57 wt% (Table 1). In contrast, the stretching behavior of the NCG/PPy aerogels changed drastically by PPy hybridization; that is, the composites became stiff and brittle, giving an ε_b of 2–3%, without large, yielding deformation seen for NCG aerogel, with an ε_b of 26%. The Young's moduli of the hydrogels and aerogels were determined as 5.3 MPa and 127 MPa, respectively, for the NCG, and 8.1 MPa and 197 MPa, respectively, for the NCG/PPy-3 composite, thus indicating that the addition of PPy had a slight stiffening effect.

The compression behavior of the aerogels (Figure 4b) also showed the stiffening effect of PPy hybridization. In this case, the change was more systematic, but highly nonlinear with regard to the PPy content. This behavior is presumably related to the percolation of the PPy phase, that is, the complete coverage of cellulose fibrils by PPy. The compression moduli of the NCG/PPy aerogels ranged from 64 to 164 MPa (Table 1), which is almost three orders of magnitude higher than those of bacterial cellulose composite aerogels (0.15 to 0.19 MPa).[8f,23] Notable in the mechanical characterization is the asymmetry between tensile and compressive behavior. Possible causes of this behavior are 1) the difference in the deformation of stiff PPy nanoparticles, and 2) the possible anisotropy in the NCG structure, with the cellulose fibrils aligning along the gel surface. Nevertheless, the mechanical properties of the NCG/PPy composite gels are much higher than those of chemically polymerized PPy powder. This large difference clearly results from the difference in the nature of the aerogel component, that is, the loose aggregates of PPy nanoparticles versus the nanofibrillar

network of cellulose based on the entanglement and intermolecular association.

We observed that the electrical conductivity of the NCG/PPy composite gels increased abruptly at a PPy content of 57 wt%, probably as a result of the formation of the continuous PPy network. The electrical conductivity of PPy is known to be enhanced by the surfactant dodecylbenzenesulfonic acid (DBSA), which reduces the interchain hopping between PPy chains.[24] The conductivity of the NCG/PPy-3 composite gels doped with DBSA was 0.08 $S\,cm^{-1}$, which is 10 times higher than that of polycaprolactone fumarate/PPy (6 $mS\,cm^{-1}$)[7f] and higher than that of bacterial cellulose/polyaniline (0.04 $S\,cm^{-1}$),[8f] which is sufficient for application in biological systems.[7a,e,25]

The high porosity and large surface area of the NCG/PPy composite aerogels allow the absorbance of aqueous liquids upon rewetting, and the recovery of the mechanical stability of the hydrogels as demonstrated in Figure 1. It can offer an environment analogous to the extracellular matrix and thus benefit the adhesion and proliferation of cells.[6b,7c] In the repair of peripheral nerve injuries, flecked tissue can be formed at the cut ends because of glia and connective-tissue hyperplasia, which prevents the recovery of function of the regenerative nerve fibers.[26] So it is necessary to use biological material as a bridge to prevent the excessive growth of connective tissue at the lesions. The PC12 cell line is an immortalized cell line derived from a neuroendocrine tumor in the rat adrenal medulla.[27] Many studies proved that the PC12 cell line is an important model system for studying the biological performance of nerve repair materials, including biocompatibiliy, cytotoxity, neural differentiation.[27,28] Thus, we chose the PC12 cell line as a model system for evaluating the biological performance of NCG/PPy composite gels as nerve-tissue repair materials, including their in vitro cytotoxicity and neural differentiation ability. Figure 5 shows that incorporation of PPy into NCGs enhances PC12 cells adhesion and proliferation on the surface of NCG/PPy composites. Significant differences were observed after three days for the NCG/PPy-3 composite and after five days for all NCG/PPy composites in the absence of DBSA. PC12 cells have a great proliferation rate on the surface of NCG/PPy composites with higher PPy content. In contrast, doping of the NCG/PPy-3 composite with DBSA slightly decreased the PC12 cell adhesion and proliferation. Moreover, the NCG/PPy-3-DBSA2 composite doped with DBSA during the final polymerization cycles were superior to the NCG/PPy-3-DBSA1 composite doped during each polymerization cycle. This observation can in part be attributed to the inhibition of protein adsorption by the high DBSA content in the composite, and the change in surface charge affecting the cell adhesion to the composites.[7e] Compared with the NCG, the NCG/PPy-3 composite shows almost the same cell proliferation rate after doping with DBSA, while maintaining good mechanical properties and no cytotoxicity.

Figure 6 shows the morphology and neurite extension from PC12 cells cultured on the NCG and NCG/PPy composites under electrical stimulation. Most of PC12 cells cultured on NCG, NCG/PPy-1, and NCG/PPy-2 composites have round morphologies, indicating virtually no neurite extension from the cell (Figure 6a–c). As expected, the cells cultured on the NCG/PPy-3 composite extended multiple longer neurites without or with dopant (Figure 6d,e), most probably because the conductivity of the composites increased with the formation of a PPy network. Moreover, it appears that the cellular morphologies of PC12 cells showed a remarkable neuronal phenotype on the surface of NCG/PPy-3 composite doped with DBSA after the final polymerization cycles (Figure 6f). The nerve guidance conduits can be prepared from NCG/PPy composites to support cell adhesion and growth on the internal surface. Under electrical stimulation, the nerve conduits that possess a similar conductive function as nerve myelin sheath can stimulate the outgrowth of nerves and axon regeneration, and finally achieve the repair of nerve injuries.[29] Thus, NCG/PPy composites are potentially useful as nerve-tissue repair materials with high mechanical stability.

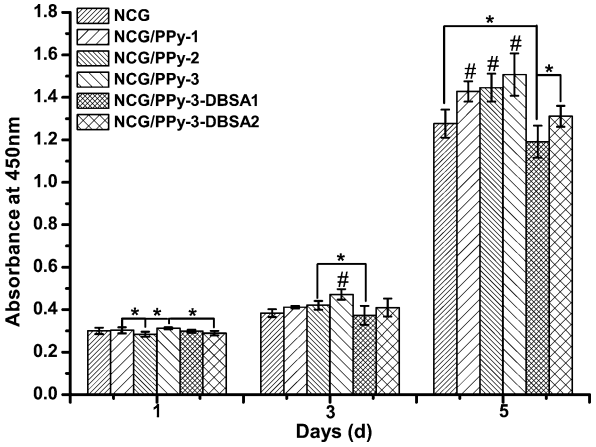

Figure 5. CCK-8 assay showing differences in cell viability of PC12 on NCG and NCG/PPy composites without or with DBSA dopant (# indicates a significant difference with the other groups, but there is no significant difference between *).

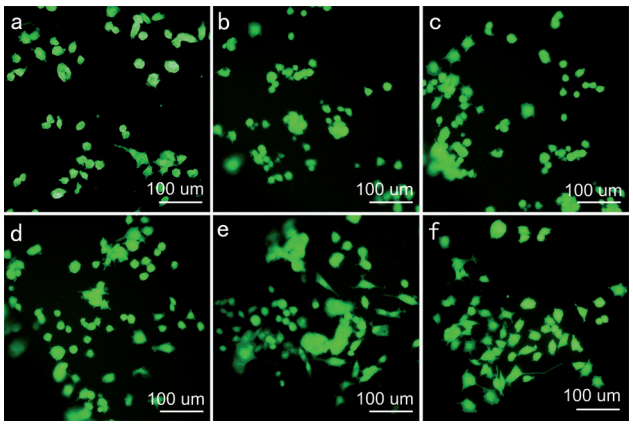

Figure 6. Fluorescence micrographs of PC12 cells cultured on different composite gels after electrical stimulation: a) NCG, b) NCG/PPy-1, c) NCG/PPy-2, d) NCG/PPy-3, e) NCG/PPy-3-DBSA1, and f) NCG/PPy-3-DBSA2.

In summary, NCGs prepared from an aqueous alkali/urea solution served as scaffold/template in the preparation of electrically conductive NCG/PPy composites by in situ vapor-phase polymerization of pyrrole monomers and an oxidant. The resulting NCG/PPy hydrogels were converted to aerogels by solvent-exchanging with ethanol and drying with supercritical CO_2, resulting in materials with a low density, a large surface area, a high mechanical strength, and sufficient electrical conductivity. In vitro studies show that PC12 cells cultured on NCG/PPy composites have good adhesion and proliferation. Furthermore, the cellular morphologies of PC12 cells show a remarkable neuronal phenotype on the surface of NCG/PPy composite doped with DBSA under electrical stimulation. The simplicity of the process and the wide tunability of the composition and thus the properties of these materials make them promising candidates for applications in nerve regeneration, carbon capture, catalyst supports, and many others.

Received: February 24, 2014
Published online: April 7, 2014

Keywords: cell adhesion · conducting materials · gels · nanoparticles · renewable resources

[1] a) J. B. Xia, L. Chen, S. Yanagida, *J. Mater. Chem.* **2011**, *21*, 4644 – 4649; b) S. S. Jeon, C. Kim, J. Ko, S. S. Im, *J. Mater. Chem.* **2011**, *21*, 8146 – 8151.

[2] a) C. Wang, W. Zheng, Z. Yue, C. O. Too, G. G. Wallace, *Adv. Mater.* **2011**, *23*, 3580 – 3584; b) J. F. Zang, X. D. Li, *J. Mater. Chem.* **2011**, *21*, 10965 – 10969.

[3] a) H. Yoon, S. H. Lee, O. S. Kwon, H. S. Song, E. H. Oh, T. H. Park, J. Jang, *Angew. Chem.* **2009**, *121*, 2793 – 2796; *Angew. Chem. Int. Ed.* **2009**, *48*, 2755 – 2758; b) O. S. Kwon, J. Y. Hong, S. J. Park, Y. Jang, J. Jang, *J. Phys. Chem. C* **2010**, *114*, 18874 – 18879; c) H. Dong, X. D. Cao, C. M. Li, *ACS Appl. Mater. Interfaces* **2009**, *1*, 1599 – 1606.

[4] V. Chandra, K. S. Kim, *Chem. Commun.* **2011**, *47*, 3942 – 3944.

[5] M. Sevilla, P. Valle-Vigon, A. B. Fuertes, *Adv. Funct. Mater.* **2011**, *21*, 2781 – 2787.

[6] a) Z. Liu, Y. Liu, S. Poyraz, X. Zhang, *Chem. Commun.* **2011**, *47*, 4421 – 4423; b) N. K. Guimard, N. Gomez, C. E. Schmidt, *Prog. Polym. Sci.* **2007**, *32*, 876 – 921.

[7] a) B. C. Thompson, S. E. Moulton, R. T. Richardson, G. G. Wallace, *Biomaterials* **2011**, *32*, 3822 – 3831; b) S. Kim, W. K. Oh, Y. S. Jeong, J. Y. Hong, B. R. Cho, J. S. Hahn, J. Jang, *Biomaterials* **2011**, *32*, 2342 – 2350; c) G. Kang, R. B. Borgens, Y. Cho, *Langmuir* **2011**, *27*, 6179 – 6184; d) W. Zheng, J. M. Razal, P. G. Whitten, R. Ovalle-Robles, G. G. Wallace, R. H. Baughman, G. M. Spinks, *Adv. Mater.* **2011**, *23*, 2966 – 2970; e) M. B. Runge, M. Dadsetan, J. Baltrusaitis, T. Ruesink, L. Lu, A. J. Windebank, M. J. Yaszemski, *Biomacromolecules* **2010**, *11*, 2845 – 2853; f) M. B. Runge, M. Dadsetan, J. Baltrusaitis, A. M. Knight, T. Ruesink, E. A. Lazcano, L. Lu, A. J. Windebank, M. J. Yaszemski, *Biomaterials* **2010**, *31*, 5916 – 5926.

[8] a) G. Nyström, A. Razaq, M. Stromme, L. Nyholm, A. Mihranyan, *Nano Lett.* **2009**, *9*, 3635 – 3639; b) S. Y. Liew, W. Thielemans, D. A. Walsh, *J. Phys. Chem. C* **2010**, *114*, 17926 – 17933; c) H. Olsson, G. Nystrom, M. Stromme, M. Sjodin, L. Nyholm, *Electrochem. Commun.* **2011**, *13*, 869 – 871; d) G. Nyström, A. Mihranyan, A. Razaq, T. Lindstrom, L. Nyholm, M. Stromme, *J. Phys. Chem. B* **2010**, *114*, 4178 – 4182; e) X. W. Shi, L. Zhang, J. Cai, G. Z. Cheng, H. M. Zhang, J. Li, X. H. Wang, *Macromolecules* **2011**, *44*, 4565 – 4568; f) M. Pääkkö, J. Vapaavuori, R. Silvennoinen, H. Kosonen, M. Ankerfors, T. Lindström, L. A. Berglund, O. Ikkala, *Soft Matter* **2008**, *4*, 2492 – 2499; g) J. G. Huang, I. Ichinose, T. Kunitake, *Chem. Commun.* **2005**, 1717 – 1719; h) C. Sasso, E. Zeno, M. Petit-Conil, D. Chaussy, M. N. Belgacem, S. Tapin-Lingua, D. Beneventi, *Macromol. Mater. Eng.* **2010**, *295*, 934 – 941.

[9] J. Foroughi, G. M. Spinks, G. G. Wallace, *J. Mater. Chem.* **2011**, *21*, 6421 – 6426.

[10] T. M. Higgins, S. E. Moulton, K. J. Gilmore, G. G. Wallace, M. I. H. Panhuis, *Soft Matter* **2011**, *7*, 4690 – 4695.

[11] S. Pruneanu, S. A. F. Al-Said, L. Q. Dong, T. A. Hollis, M. A. Galindo, N. G. Wright, A. Houlton, B. R. Horrocks, *Adv. Funct. Mater.* **2008**, *18*, 2444 – 2454.

[12] J. F. Beecher, *Nat. Nanotechnol.* **2007**, *2*, 466 – 467.

[13] a) T. Nishino, I. Matsuda, K. Hirao, *Macromolecules* **2004**, *37*, 7683 – 7687; b) S. Eichhorn, A. Dufresne, M. Aranguren, N. Marcovich, J. Capadona, S. Rowan, C. Weder, W. Thielemans, M. Roman, S. Renneckar, *J. Mater. Sci.* **2010**, *45*, 1 – 33.

[14] J. Cai, S. Kimura, M. Wada, S. Kuga, L. Zhang, *ChemSusChem* **2008**, *1*, 149 – 154.

[15] a) J. Cai, S. Kimura, M. Wada, S. Kuga, *Biomacromolecules* **2009**, *10*, 87 – 94; b) J. Cai, S. L. Liu, J. Feng, S. Kimura, M. Wada, S. Kuga, L. Zhang, *Angew. Chem.* **2012**, *124*, 2118; *Angew. Chem. Int. Ed.* **2012**, *51*, 2076.

[16] Q. Y. Wang, J. Cai, L. N. Zhang, M. Xu, H. Cheng, C. C. Han, S. Kuga, J. Xiao, R. Xiao, *J. Mater. Chem. A* **2013**, *1*, 6678 – 6686.

[17] V. Estévez, M. Villacampa, J. C. Menéndez, *Chem. Soc. Rev.* **2010**, *39*, 4402.

[18] A. Laforgue, L. Robitaille, *Macromolecules* **2010**, *43*, 4194.

[19] Y. Maréchal, H. Chanzy, *J. Mol. Struct.* **2000**, *523*, 183 – 196.

[20] P. Jha, S. P. Koiry, V. Saxena, P. Veerender, A. K. Chauhan, D. K. Aswal, S. K. Gupta, *Macromolecules* **2011**, *44*, 4583 – 4585.

[21] S. J. Eichhorn, W. W. Sampson, *J. R. Soc. Interface* **2005**, *2*, 309 – 318.

[22] J. Stejskal, M. Trchova, S. Fedorova, I. Sapurina, J. Zemek, *Langmuir* **2003**, *19*, 3013 – 3018.

[23] R. T. Olsson, M. A. A. Samir, G. Salazar-Alvarez, L. Belova, V. Strom, L. A. Berglund, O. Ikkala, J. Nogues, U. W. Gedde, *Nat. Nanotechnol.* **2010**, *5*, 584 – 588.

[24] M. Kotal, S. K. Srivastava, B. Paramanik, *J. Phys. Chem. C* **2011**, *115*, 1496 – 1505.

[25] a) S. S. Mihardja, R. E. Sievers, R. J. Lee, *Biomaterials* **2008**, *29*, 4205 – 4210; b) J. Y. Lee, C. A. Bashur, A. S. Goldstein, C. E. Schmidt, *Biomaterials* **2009**, *30*, 4325 – 4335.

[26] a) M. T. Fitch, J. Silver, *Exp. Neurol.* **2008**, *209*, 294 – 301; b) Y. Nishimura, A. Natsume, M. Ito, M. Hara, K. Motomura, R. Fukuyama, N. Sumiyoshi, I. Aoki, T. Saga, H. J. Lee, T. Wakabayashi, S. U. Kim, *Cell Transplantation* **2013**, *22*, 2187 – 2201.

[27] L. A. Greene, A. S. Tischler, *Proc. Natl. Acad. Sci. USA* **1976**, *73*, 2424 – 2428.

[28] a) J. D. Foley, E. W. Grunwald, P. F. Nealey, C. J. Murphy, *Biomaterials* **2005**, *26*, 3639 – 3644; b) B. Li, Y. Ma, S. Wang, P. M. Moran, *Biomaterials* **2005**, *26*, 1487 – 1495; c) C. M. O'Driscoll, A. M. Gorman, *Neuroscience* **2005**, *131*, 321 – 329.

[29] a) J. Xie, M. R. MacEwan, S. M. Willerth, X. Li, D. W. Moran, S. E. Sakiyama-Elbert, Y. Xia, *Adv. Funct. Mater.* **2009**, *19*, 2312 – 2318; b) H. Xu, J. M. Holzwarth, Y. Yan, P. Xu, H. Zheng, Y. Yin, S. P. Li, P. X. Ma, *Biomaterials* **2014**, *35*, 225 – 235.

